ECS Journal of Solid State Science and Technology, **8** (12) M111-M117 (2019)
2162-8769/2019/8(12)/M111/7/$38.00 © The Electrochemical Society

First Principles Study of the Ambipolarity in a Germanene Nanoribbon Tunneling Field Effect Transistor

Azam Samipour,[1] Daryoosh Dideban,[1,z] and Hadi Heidari[2]

[1] *Institute of Nanoscience and Nanotechnology, University of Kashan, Kashan, Iran*
[2] *James Watt School of Engineering, University of Glasgow, G12 8QQ, Glasgow, United Kingdom*

In this article, the effects of hetero-dielectric gate material and gate-drain underlap on the ambipolar and ON-state current of a germanene nanoribbon (GeNR) tunneling field-effect transistors (TFETs) is examined. The simulations are performed using the combination of density functional theory (DFT) and non-equilibrium Green's function (NEGF) formalism. It was observed that using high-k dielectric gate material increases the ON-state current while the combination of hetero-dielectric gate material and gate-drain underlap suppresses the ambipolar current and improves the ON-state current. In addition, the effect of various hetero-junctions in the source region on the performance of GeNR-TFET was investigated. Due to the dependency between the width and energy bandgap in GeNR, utilizing a small bandgap in the source improves ON-state current and its ambipolar behavior.
 [DOI: 10.1149/2.0021912jss]

Manuscript submitted October 14, 2019; revised manuscript received November 13, 2019. Published November 25, 2019.

In order to continue performance improvement of Metal-Oxide-Semiconductor fielde effect transistors (MOSFETs), their dimensions have been scaled down continuously in the last decades and it is reached to less than 10 nm now. However, this matter has led to a significant increase in power consumption. Due to aggressive shrinking of the device dimensions, short-channel effects such as drain induced barrier lowering (DIBL) are increased resulting in worse leakage current. On the other hand, the fundamental theoretical limit of the subthreshold swing (SS), which is about 60 mV/dec at room temperature for conventional MOSFETs, does not permit further decrease of the leakage current in these devices. Therefore alternative device structures and materials are proposed to overcome these problems.[1–7] They could offer a subthreshold swing (SS) smaller than 60 mV/dec.[2] In recent years special attention has been paid to novel 2D materials and in particular to graphene, silicene and germanene because of their unique electronic, mechanical and optical properties. They offer a great potential for future nanoelectronic device applications.[8–11]

These materials are two-dimensional with a hexagonal honeycomb structure. There is a Dirac point and a linear electronic dispersion around this point in these materials. They belong to group IV of the periodic table. Graphene is comprised of sp^2 hybridized carbon atoms and planar configuration whereas silicene and germanene because to the mixing of sp^2 and sp^3 hybridization have low-buckled structure.[10–18] Various studies show that graphene, germanene and silicene monolayers have zero bandgap. Since in electronic devices, semiconductor materials with a tunable bandgap is required it was necessary to overcome this issue. Utilizing these materials as nanoribbons with a desired width yields a non-zero bandgap which is tunable.[8,11,12,19–21] Graphene, germanene and silicene nanoribbons are candidates for next generation devices due to significant electronic properties such as direct bandgap and light carrier effective mass,[2,22–24] high carrier mobility and high current density.[23,25–27]

On the other hand, TFETs which are based on interband tunneling mechanism have attracted much interest. TFETs have advantages such as subthreshold swing below 60mV/dec, less leakage current and better immunity to short channel effects (SCEs). However, disadvantages are also observed, such as less on-current (I_{ON}) than a high performance MOSFET and ambipolar behavior in TFETs. Ambipolarity means that depending on the type of voltage applied, tunneling happens in two directions. In n-channel TFETs, for instance, by applying positive gate voltage, electrons tunnel from the source to the channel that this results in an on-state current (I_{ON}) while by applying a negative gate voltage, hole tunneling occurs from the drain to the channel that results in an ambipolar current (I_{amb}).

This problem degrades the switching characteristics and makes the TFET less efficient for digital circuit design. In order to overcome these issues, several methods have been introduced. The most important among them are use of high-k gate dielectric, multiple-gate structure, hetero-dielectric gate (HG), gate-drain overlap, heterojunction TFETs, drain underlap, band-gap engineered TFETs and drain doping engineering.[28–36]

In this paper, the effect of hetero-dielectric and a gate-drain underlap on the ambipolar characteristics and ON-state current in a GeNR-TFET is investigated. Moreover, the effect of changing the source bandgap on the performance of this device is evaluated.

Device Structure and Simulation Setup

The electronic properties and current-voltage characteristics were investigated utilizing the density functional theory (DFT) and non-equilibrium Green's function (NEGF) method in the Atomistic ToolKit -Virtual Nanolab (ATK-VNL).[37]

The exchange correlation employed is the Generalized Gradient Approximation (GGA) of Perdew–Burke–Ernzerhof (PBE) functional.The cutoff energy and a Monkhorst-Pack k-point are considered 80 Hartree and $1 \times 1 \times 51$, respectively. Hartwigsen–Goedecker–Hutter (HGH) pseudopotential is applied as basis set.[10]

Periodic boundary conditions with vacuum layer of approximately 15 Å for each side of the unitcell are employed to prevent undesired image-image interaction. It is worth noting that the vacuum layer size for the AGeNR case is in agreement with the previous works presented in Refs. 38,39.

To remove the dangling bond effects on the surface of nanoribbons, edges on both sides were passivated with hydrogen atoms. In order to obtain the optimum structure, the initial defined structure is relaxed until the maximum atomic force to each atom smaller than 0.02 eV/Å is obtained. The $1 \times 1 \times 101$ k-points have been used to obtain electronic properties. Moreover, the temperature is set at $T = 300$ K.[10,38] Fig. 1 illustrates the armchair GeNR unit cell. The bond length of Ge–Ge and parameter of buckling was obtained 2.4 Å and $\Delta = 0.67$ Å, respectively.

I–V characteristic behavior under a drain-source voltage (V_{bias}) and gate voltage (V_g) is calculated as:

$$I\left(V_g, V_{bias}\right) = \frac{2e}{h}\int_{-\infty}^{+\infty}\{Tr[\Gamma_L G^R \Gamma_R G^A] \times [f_L\left(E-\mu_L\right) - f_R\left(E-\mu_R\right)]\}dE \quad [1]$$

where e, h, Γ, $f_{L/R}$ and $\mu_{L/R}$ are electron charge, Planck's constant, contact broadening function of left(L) and right(R) electrodes, Fermi–Dirac distribution function of L/R electrodes and chemical potential of L/R electrode, respectively. Furthermore G is the Green's function

[z] E-mail: dideban@kashanu.ac.ir

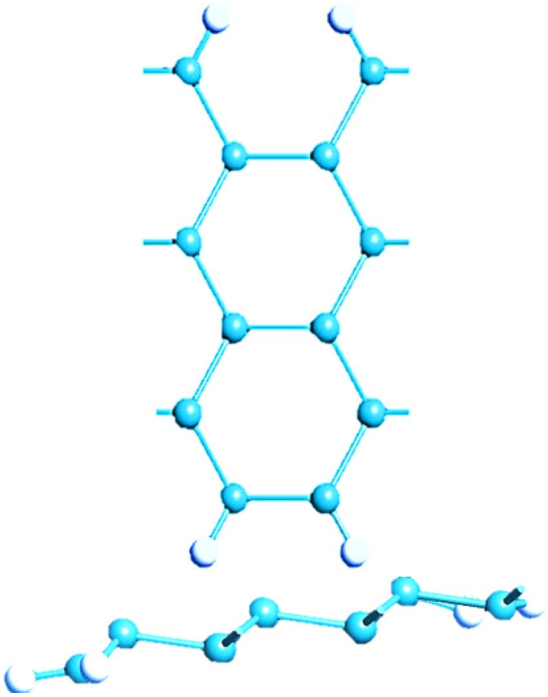

Figure 1. Top and side views of the relaxed 6-AGeNR.

of device that is given by:

$$G_d = \left(E - H_d - \sum\nolimits_L - \sum\nolimits_R\right)^{-1} \quad [2]$$

where E, H_d and $\Sigma_{L/R}$ are carrier energy, the Hamiltonian of device and the self-energy of L/R electrodes, respectively[40,41]

Fig. 2 shows the schematic of proposed GeNR-TFET. The p-i-n GeNR tunneling FET has a 10-nm long GeNR channel with index of N = 6, where N is the number of atoms along the ribbon width. The gate insulators used in this study are SiO_2(K = 4) and HfO_2(K = 25) with 1.5 nm thickness and the gate metal thickness is 0.5 nm. The source and drain lengths are the same and equal to 7.04 Å .The gate insulator covers the entire nanoribbon but the gate metal only covers the channel. The channel is undoped whereas p-type and n-type dopants are introduced into the source and drain regions, respectively. Doping value is chosen 0.8%.

The utilized power supply voltage is $V_D = 0.5V$. Lengths of the gate (L_{gate}) and channel are the same. $L_{underlap}$ is considered from the edge of the gate to the junction of the drain.

Results and Discussion

In this section the results obtained from the simulation of the device under study at room temperature are discussed. Therefore, the transfer characteristics for hetero-dielectric gate material, gate-drain underlap and hetero-junction at the source region are presented. Their performance has been investigated in terms of ON-state (I_{ON}) and ambipolar current (I_{amb}).

Impact of mono/hetero dielectric materials on the transfer characteristics.—In this subsection, impact of hetero dielectric gate on controlling the ambipolar characteristic is studied. In order to examine the obtained data, a detailed review on the formulation of the tunnel current is required. The dependence of the ON state current (I_{ON}) on the transmission probability in TFETs[35,36] is explained by:

$$I \propto T(E) = \exp\left(-\frac{4\sqrt{2m^*}E^{\frac{3}{2}}}{3|e|\hbar\left(E_g + \Delta\varphi\right)}\sqrt{\frac{\varepsilon_s}{\varepsilon_{ox}}t_{ox}t_s}\right)\Delta\varphi \quad [3]$$

where e, $\hbar$, E_g, m^* and $\Delta\varphi$ represent the electron charge, the reduced Planck's constant, the bandgap, the effective mass and the energy range of tunneling location, respectively. t_{ox} and ε_{ox} are oxide thickness and dielectric constant while t_s and ε_s denote the corresponding values for the semiconductor close to the tunnel junction.

This equation indicates that ON-state current (I_{ON}) can be increased by increasing the dielectric constant (ε_{ox}). The transfer characteristic (I_D-V_G) for the GeNR-TFET presented in Fig. 2 was calculated for two different mono-dielectrics (SiO_2 and HfO_2). The results obtained for this study are compared and shown in Fig. 3.

Despite the improvement of the ON state and OFF-state (leakage) current for high-k dielectric case (HfO_2), Fig. 3 indicates that the ambipolar current in the GeNR-TFET utilizing HfO_2 dielectric is more. In order to overcome this problem, we examined the idea of using a different combination of high dielectric (HfO_2) and low dielectric (SiO_2) insulators at the source/drain sides of the channel. Fig. 4 compares the transfer characteristics at $V_D = 0.5V$ for the devices utilizing hetero-dielectric materials which is comprised of a combination of SiO_2 and HfO_2 in three cases:

a) Three-fourths of the dielectric length made from low-k material (SiO_2) and is located at the drain side and one-fourth of that made from high-k material (HfO_2) which is located at the source side.
b) Both sizes of high-k and low-k dielectrics are equal.
c) One-fourth of dielectric length made from SiO_2 and is located at the drain side and three-fourths of that made from HfO_2which is located at the source side.

It is worth noting that in all three cases, high-k/ low-k materials are located close to the source/drain sides, respectively. In other words, the dielectric in the drain side is SiO_2 while the dielectric in the source side is HfO_2.

According to Fig. 4, case *c* which utilizes more HfO_2 at the source side gives more ON-state current (I_{ON}). This is in agreement with what we expect from Equation 3 because occurrence of more tunneling necessitates use of high-k material in the source side. Furthermore, the use of higher dielectric material with an increased length leads to more electrostatic coupling between the gate and the junction of source/channel resulting in the enhancement of I_{ON}.

As shown in Fig. 4, if the SiO_2 length becomes more than the length of the HfO_2 (case *a*) the ambipolar current decreases. However, it can be seen that I_{ON} is also reduced, so there is a trade-off between the ambipolar current and I_{ON}.

The sub-threshold swing (SS) is another important parameter of the field effect transistor that is calculated as $SS = dV_G/d\log(I)$.[11] It

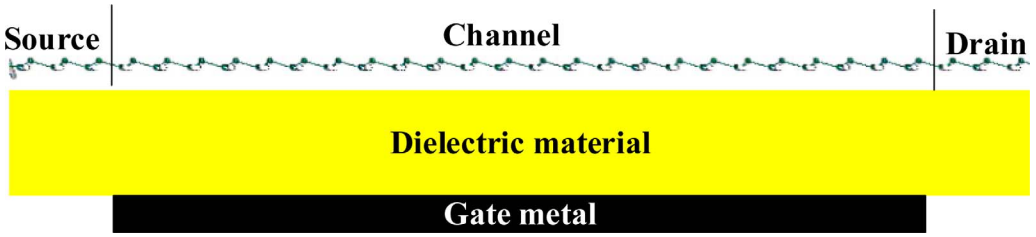

Figure 2. Schematic of a simulated GeNR TFET.

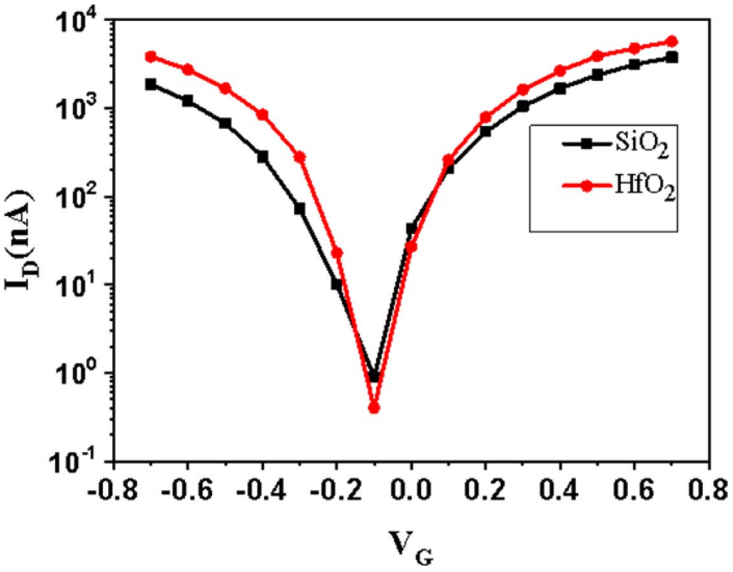

Figure 3. The current-voltage characteristics for two mono-dielectrics in GeNR-TFET under study at $V_{DS} = 0.5V$.

is desired to have a low SS value, because it leads to better switching behavior of the transistor. It is worth noting that since the drain current behavior of the tunneling devices is not linear versus the gate voltage at the subthreshold region, the SS value must be measured at a particular point and since the Dirac point has the highest slope, SS is calculated at this point.

From Fig. 3 the calculated SS is equal to 54mV/decade for TFET utilizing SiO_2 and 50 mV/decade for the case utilizing HfO_2. This indicates the use of high-k material gives better or reduced value of SS for mono-dielectric case. However, for hetero-dielectric cases shown in Fig. 4, the SS value is between these two values (50 and 54 mV/decade) and the more the length of high-k material, the less the value of SS will be.

Impact of gate-drain underlap on the transfer characteristics.— In this subsection, we would like to investigate the impact of gate underlap on the ambipolar characteristic**.** In this study the channel length is fixed at 10 nm and the gate underlap length is changed between 1 nm and 3 nm, as shown in Fig. 5.

Fig. 6 exhibits I-V characteristics for the GeNR-TFETs with various gate-drain underlaps at $V_D = 0.5$ V. As shown in Fig. 6, ambipolar characteristic is suppressed as the gate-drain underlap increases.

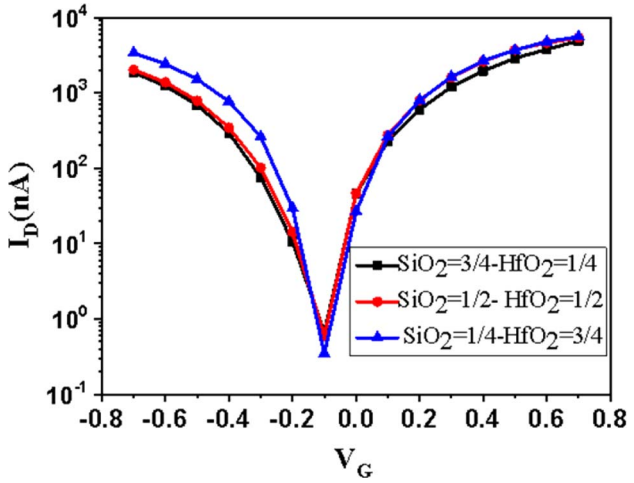

Figure 4. The current-voltage characteristics for three cases of hetero-dielectric in GeNR-TFET under study at Vds = 0.5V.

In order to investigate the origin of this observation the energy band diagram along the device length is plotted in Fig. 7.

It can be seen from Fig. 7 that the electric field generated by the gate voltage on the drain side gradually decreases as the gate underlap length increases. Due to reduction of the electric field at the drain-channel interface, the band bending is reduced and this in turn leads to an increase in the tunneling barrier width. Therefore, carrier tunneling in this interface is reduced. It is also observed that the gate-drain underlap does not have an effect on the source-channel interface. Therefore gate-drain underlap is one way of suppressing the ambipolar current. However, the length of the gate should not be so short, because by increasing the gate-drain underlap, direct current from source to drain increases and this might cause an unwanted increase in the drain current.

According to Fig. 6, it can be seen that the when the length of the underlap is 1nm, it is optimum. This is due to the fact that the ambipolar current has decreased and the off-state current has not changed. Table I shows the electronic parameters of the device under study in comparison with other published works.

Impact of source bandgap on the transfer characteristics.—Eventually, the device performance of a TFET composed of heterostructure armchair GeNR (AGeNR) with a length of 10 nm and an index of N = 6 for the channel is evaluated. For AGeNR the bandgap is determined by the width. Considering the dependency between the width and bandgap, AGeNRs are classified into three groups: N = 3m, N = 3m+1 and N = 3m+2; where N identifies the number of germanium atoms along the ribbon width, and m is a positive integer. A large, moderate and minimum bandgap belong to N = 3m+1, N = 3m, and N = 3m+2 groups, respectively. Due to strong dependence of the quantum confinement on the nanoribbon width, for AGeNR, smaller

Table I. Parameters of the optimal state of AGeNR-TFET Comparison of the main figures of merit of TFETs made of several 2D channel materials.

Parameter	This work	42	11	43
I_{ON}/I_{OFF}	10^4	1.9×10^3	10^5	-
SS (mV/decade)	52	68	11.54	-
Transconductance (gm $\mu\Omega^{-1}$) (max)	14	-	11	-
DIBL	0.2 ($V_d = 0.5V$, $V_d = 1V$)	-	-	0.5

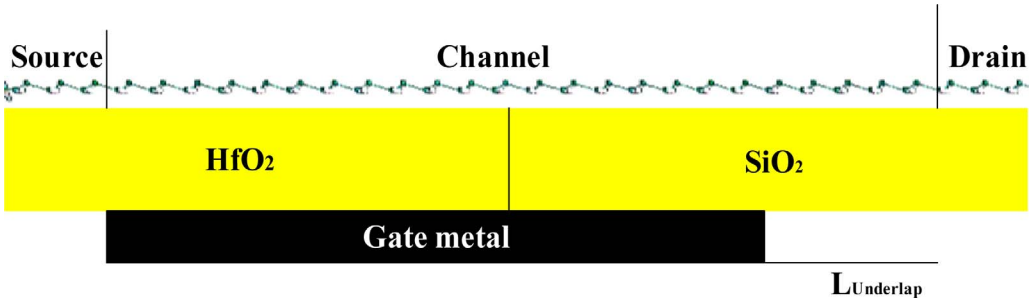

Figure 5. Schematic of GeNR-TFET with a gate-drain underlap.

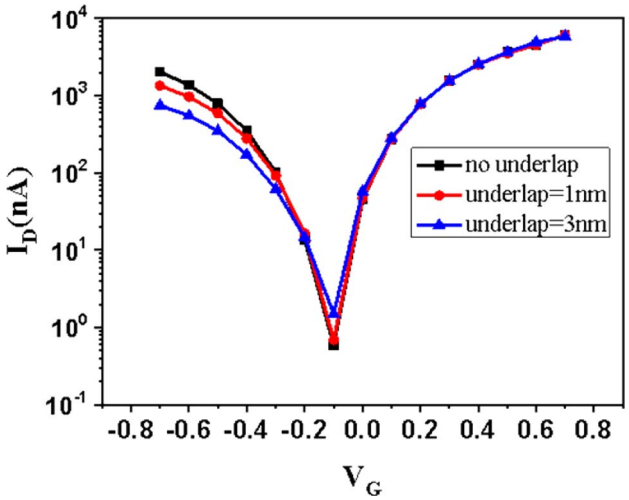

Figure 6. The current-voltage characteristics for various gate underlaps at the drain end of the channel at $V_D = 0.5$ V.

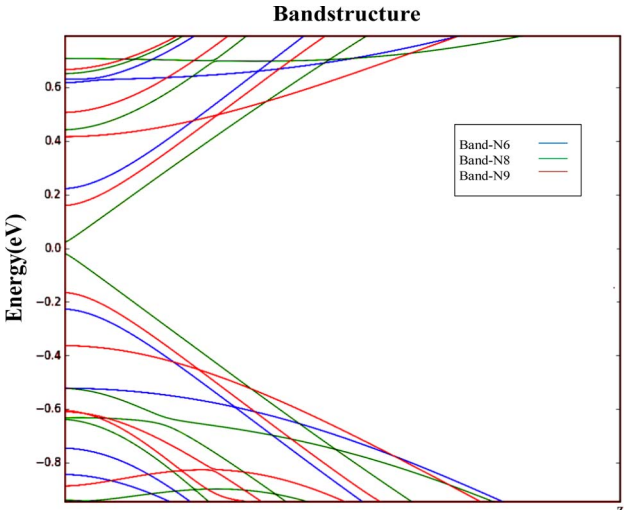

Figure 8. The band structure of three germanene nanoribbons with various widths of N = 6,8,9.

band gaps are obtained with wider ribbons.[10,44,45] Fig. 8 indicates the band structure of three germanene nanoribbons with various widths of N = 6, 8, 9.

In order to better illustrate important electronic properties of AGeNRs, we extracted the electron effective mass and the bandgap from Fig. 8. Fig. 9a shows variation in the effective mass with ribbon width (N) for the GeNRs with 6, 8 and 9 atoms along the width. As can be seen in Fig. 9a, effective mass is changed depending on the width of the nanoribbon. Ribbon with width 6 has the highest effective mass and width 8 has the least effective mass among these three widths. Also in Fig. 9b variation in bandgap energy (E_g) versus ribbon width (N) is shown. As can be seen in Fig. 9b, GeNR with width 6 has the highest bandgap and width 8 has the lowest bandgap among these three widths.

In these simulations, N = 8 and N = 9 in the source region are used because in these cases AGeNR behaves either metallic or semi-metallic. The case of N = 6 is not suitable to be used in the source region because it shows a larger bandgap around 0.4 eV as indicated in Fig. 8. The device atomic structure is shown in Fig. 10.

The transfer characteristic for AGeNR-TFET with different configurations in the source is shown in Fig. 11. Three structures were simulated using first principles calculations comprised of (a)-homo-junction with N = 6 for channel and source; (b)-hetero-junction with N = 6 for channel and drain while N = 8 for the source; (c)- hetero-junction with N = 6 for channel and drain and N = 9 for the source. From Fig. 11, it is concluded that utilizing hetero-junctions at the source (small E_g) leads to higher I_{ON} but the I_{OFF} is increased compared with the homo-junction case. To explain the general transport mechanism of the GeNR-TFETs, energy band diagrams at OFF-state and ON-state are plotted in Fig. 12.

According to Fig. 12a, at OFF-state the valence band of the source is located under the conduction band of the channel. Therefore, due to the lack of mobile carriers at the source/ drain-channel junctions, the major contributing of current is direct tunneling from source to drain. Using a smaller energy bandgap at the source reduces the effective tun-

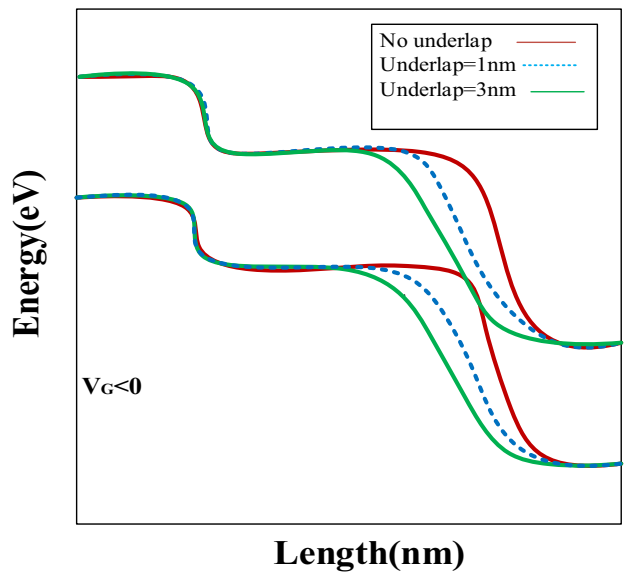

Figure 7. Band diagram in ambipolar state for different gate-drain underlaps.

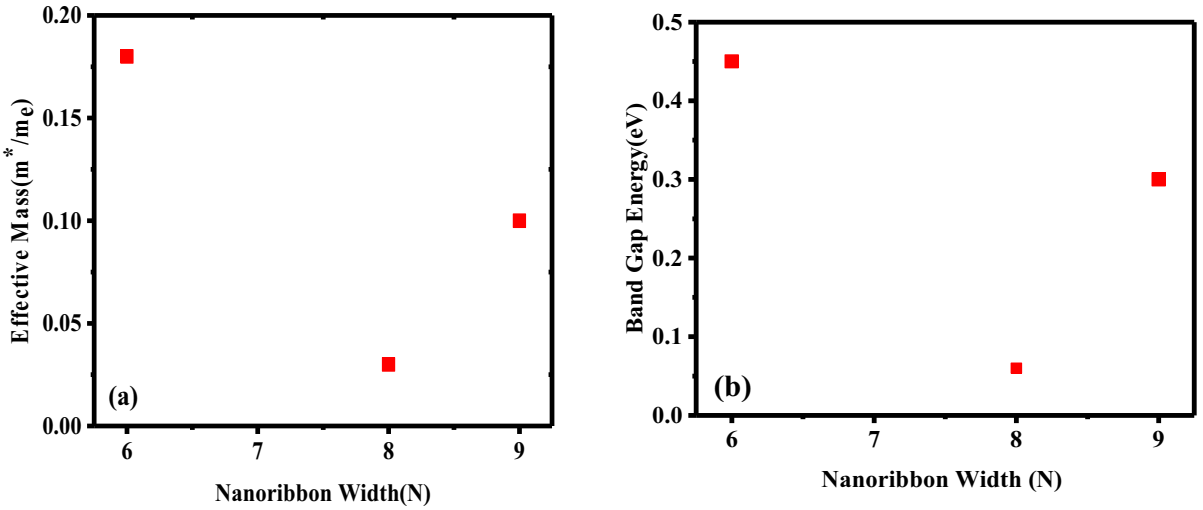

Figure 9. (a) The electron effective mass and (b) the bandgaps of GeNRs with different atoms along the width (N = 6,8,9).

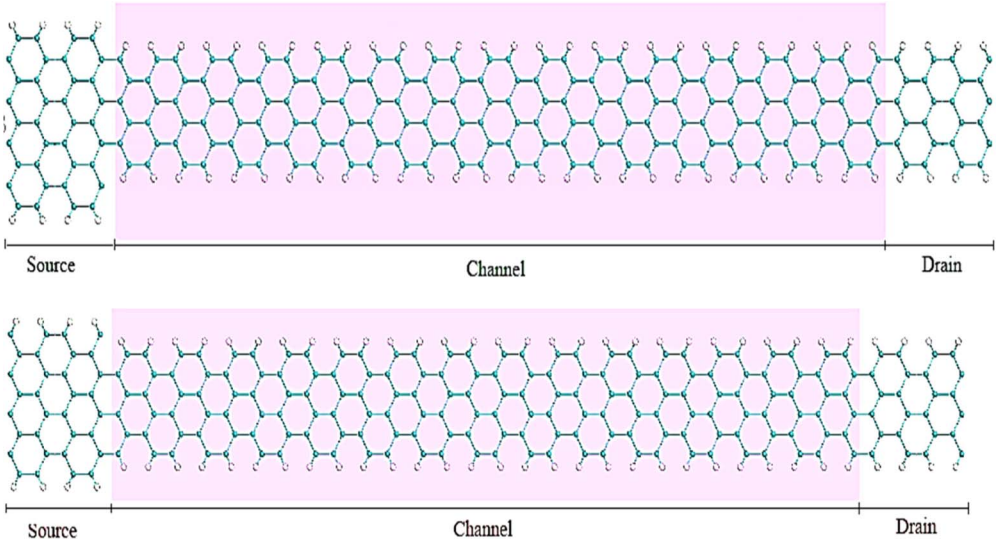

Figure 10. Atomic structure of simulated AGeNR-TFET with different widths in the source, top structure has N = 9 atoms along the source width and bottom structure has N = 8 atoms along the source width. The channel region is colored pink at the background.

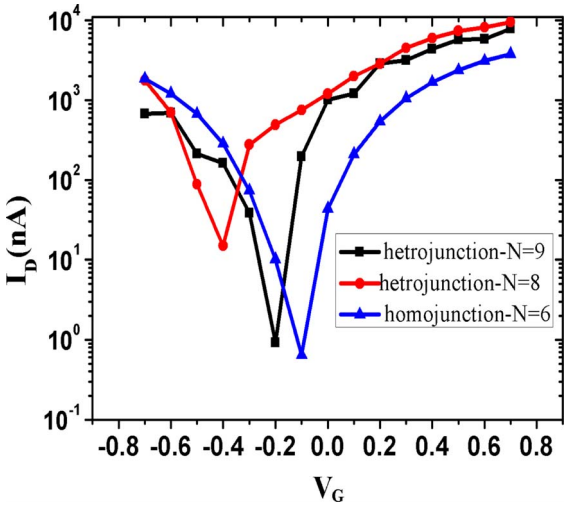

Figure 11. The current-voltage characteristics for GeNR-TFETs corresponding to N = 6, 8 and 9 atoms along the source.

neling width from the source to drain and as a result, I_{OFF} increases. Moreover, the ambipolar current has been improved, as shown in Fig. 11.

Based on energy band diagram shown in Fig. 12b, at ON-state the valence band of the source is located upper than the conduction band of the channel. It can be seen that due to insertion of smaller E_G material in the source region, a sharper profile will be created in the source/channel junction and hetero-junction has a thinner tunneling barrier compared with homo-junction. As a result, the probability of carrier tunneling will be higher and the ON-state current becomes larger. Another factor in the improvement of ON-state current is the increase in tunneling area due to the presence of materials with smaller bandgap in the source. This means that more electrons contribute to the band-to-band tunneling.

As a result, as the width of AGeNR in the source is increased, energy bandgap becomes smaller and the tunneling current increases. This is in agreement with the enhanced value of on-state current of hetero-junction with N = 8 compared with on-state current of its counterpart having N = 9. However, the ambiploar current will be worse in this case. Among these three cases, the overall behavior of the transfer characteristic will be better for N = 9 case, where the ambipolar

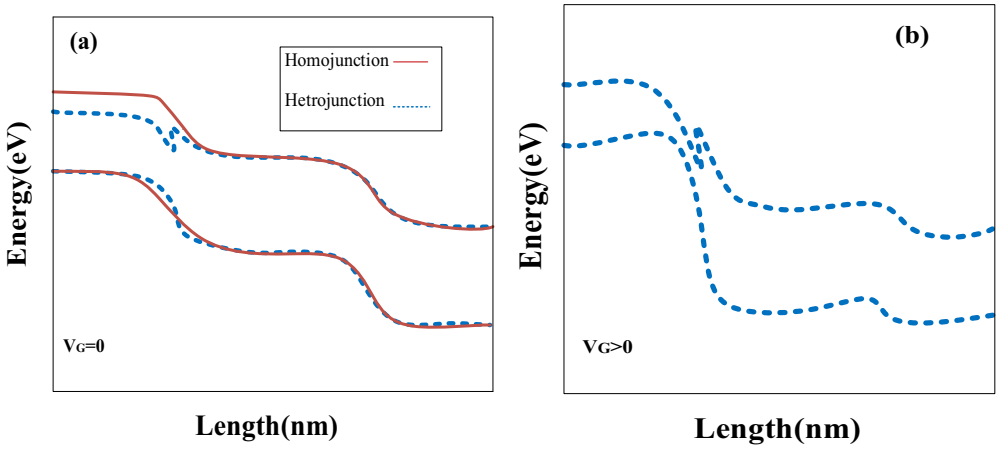

Figure 12. Energy band diagram for hetero-junction case at (a) OFF state and (b) ON state.

current is one order of magnitude less than the ON-state current as indicated in Fig. 11.

Conclusions

In this article, a back-gated GeNR tunneling field effect transistor is proposed and its ambipolar current and ON-state current were theoretically studied. Due to the undesirable effects of the ambipolar current on digital electronic applications, it was shown that the use of hetero-dielectric material as well as a gate underlap leads to improved performance of the device in terms of ambipolar current and ON-state current. Moreover, performance of a GeNR-TFET with various hetero-junctions in the source/channel interface was studied. Utilizing a wide ribbon with smaller bandgap in the source led to narrower tunneling width and an increase of the tunneling area. Therefore, I_{ON} and ambipolar current were improved.

Acknowledgments

This research was supported by University of Kashan under supervision of Dr. Daryoosh Dideban. Authors are thankful to the support received for this work from Micoelectronics Lab (meLab) at the University of Glasgow, UK.

ORCID

Daryoosh Dideban https://orcid.org/0000-0002-6645-1344

References

1. E.-H. Toh, G. H. Wang, G. Samudra, and Y.-C. Yeo, "Device physics and design of germanium tunneling field-effect transistor with source and drain engineering for low power and high performance applications," *Journal of Applied Physics*, **103**, 104504, (2008).
2. P. Zhao, J. Chauhan, and J. Guo, "Computational study of tunneling transistor based on graphene nanoribbon," *Nano letters*, **9**, 684, (2009).
3. D. S. Yadav, D. Sharma, B. R. Raad, and V. Bajaj, "Impactful study of dual work function, underlap and hetero gate dielectric on TFET with different drain doping profile for high frequency performance estimation and optimization," *Superlattices and Microstructures*, **96**, 36, (2016).
4. A. S. Verhulst, W. G. Vandenberghe, K. Maex, and G. Groeseneken, "Tunnel field-effect transistor without gate-drain overlap," *Applied Physics Letters*, **91**, 053102, (2007).
5. M. S. Sarker, M. M. Islam, M. N. K. Alam, and M. R. Islam, "Gate dielectric strength dependent performance of CNT MOSFET and CNT TFET: A tight binding study," *Results in physics*, **6**, 879, (2016).
6. R. Huang, Q. Huang, S. Chen, C. Wu, J. Wang, X. An et al., "High performance tunnel field-effect transistor by gate and source engineering," *Nanotechnology*, **25**, 505201, (2014).
7. G. Han, P. Guo, Y. Yang, L. Fan, Y. S. Yee, C. Zhan et al., "Source engineering for tunnel field-effect transistor: Elevated source with vertical silicon–germanium/germanium heterostructure," *Japanese Journal of Applied Physics*, **50**, 04DJ07, (2011).
8. M. Zoghi, A. Y. Goharrizi, and M. Saremi, "Band gap tuning of armchair graphene nanoribbons by using antidotes," *Journal of Electronic Materials*, **46**, 340, (2017).
9. C. Clendennen, N. Mori, and H. Tsuchiya, "Non-equilibrium Green function simulations of graphene, silicene, and germanene nanoribbon field-effect transistors," *Journal of Advanced Simulation in Science and Engineering*, **2**, 171, (2015).
10. M. Monshi, S. Aghaei, and I. Calizo, "Edge functionalized germanene nanoribbons: impact on electronic and magnetic properties," *RSC Advances*, **7**, 18900, (2017).
11. A. H. Bayani, D. Dideban, M. Vali, and N. Moezi, "Germanene nanoribbon tunneling field effect transistor (GeNR-TFET) with a 10 nm channel length: analog performance, doping and temperature effects," *Semiconductor Science and Technology*, **31**, 045009, (2016).
12. H. Da, K.-T. Lam, G. S. Samudra, G. Liang, and S.-K. Chin, "Influence of contact doping on graphene nanoribbon heterojunction tunneling field effect transistors," *Solid-State Electronics*, **77**, 51, (2012).
13. A. Acun, L. Zhang, P. Bampoulis, M. Farmanbar, A. van Houselt, A. Rudenko et al., "Germanene: the germanium analogue of graphene," *Journal of Physics: Condensed Matter*, **27**, 443002, (2015).
14. S. Trivedi, A. Srivastava, and R. Kurchania, "Silicene and germanene: a first principle study of electronic structure and effect of hydrogenation-passivation," *Journal of Computational and Theoretical Nanoscience*, **11**, 781, (2014).
15. S.-S. Li, C.-W. Zhang, W.-X. Ji, F. Li, P.-J. Wang, S.-J. Hu et al., "Tunable electronic and magnetic properties in germanene by alkali, alkaline-earth, group III and 3d transition metal atom adsorption," *Physical Chemistry Chemical Physics*, **16**, 15968, (2014).
16. Z. Ni, Q. Liu, K. Tang, J. Zheng, J. Zhou, R. Qin et al., "Tunable bandgap in silicene and germanene," *Nano Letters*, **12**, 113, (2011).
17. T. P. Kaloni and U. Schwingenschlögl, "Stability of germanene under tensile strain," *Chemical Physics Letters*, **583**, 137, (2013).
18. Y. Wang, J. Zheng, Z. Ni, R. Fei, Q. Liu, R. Quhe et al., "Half-metallic silicene and germanene nanoribbons: toward high-performance spintronics device," *Nano*, **7**, 1250037, (2012).
19. S. Singh, K. Garg, A. Sareen, R. Mehla, and I. Kaur, "Doped armchair germanene nanoribbon exhibiting negative differential resistance and analysing its nano-FET performance," *Organic Electronics*, **54**, 261, (2018).
20. W. Zhang, C. Basaran, and T. Ragab, "Impact of geometry on transport properties of armchair graphene nanoribbon heterojunction," *Carbon*, **124**, 422, (2017).
21. Y. Lv, Q. Huang, H. Wang, S. Chang, and J. He, "A numerical study on graphene nanoribbon heterojunction dual-material gate tunnel FET," *IEEE electron device letters*, **37**, 1354, (2016).
22. Q. Zhang, T. Fang, H. Xing, A. Seabaugh, and D. Jena, "Graphene nanoribbon tunnel transistors," *IEEE Electron Device Letters*, **29**, 1344, (2008).
23. A. Y. Goharrizi, M. Zoghi, and M. Saremi, "Armchair graphene nanoribbon resonant tunneling diodes using antidote and BN doping," *IEEE Transactions on Electron Devices*, **63**, 3761, (2016).
24. M. Saremi, M. Saremi, H. Niazi, and A. Y. Goharrizi, "Modeling of lightly doped drain and source graphene nanoribbon field effect transistors," *Superlattices and Microstructures*, **60**, 67, (2013).
25. K. I. Bolotin, K. J. Sikes, Z. Jiang, M. Klima, G. Fudenberg, J. Hone et al., "Ultrahigh electron mobility in suspended graphene," *Solid State Communications*, **146**, 351, (2008).
26. P. Zomer, S. Dash, N. Tombros, and B. Van Wees, "A transfer technique for high mobility graphene devices on commercially available hexagonal boron nitride," *Applied Physics Letters*, **99**, 232104, (2011).
27. K. S. Novoselov, A. K. Geim, S. Morozov, D. Jiang, M. I. Katsnelson, I. Grigorieva et al., "Two-dimensional gas of massless Dirac fermions in graphene," *nature*, **438**, 197, (2005).
28. S. Sahay and M. J. Kumar, "Controlling the drain side tunneling width to reduce ambipolar current in tunnel FETs using heterodielectric BOX," *IEEE Transactions on Electron Devices*, **62**, 3882, (2015).

29. M. Madhini and G. Saini, "Heterojunction tunnel FET with Heterodielectric BOX," in 2016 *International Conference on Communication and Signal Processing (ICCSP)*, 1743 (2016).
30. W. Li, H. Liu, S. Wang, S. Chen, and Z. Yang, "Design of high performance Si/SiGe heterojunction tunneling FETs with a T-shaped gate," *Nanoscale research letters*, **12**, 198, (2017).
31. D. B. Abdi and M. J. Kumar, "Controlling ambipolar current in tunneling FETs using overlapping gate-on-drain," *IEEE Journal of the Electron Devices Society*, **2**, 187, (2014).
32. G. Lee, J.-S. Jang, and W. Y. Choi, "Dual-dielectric-constant spacer hetero-gate-dielectric tunneling field-effect transistors," *Semiconductor Science and Technology*, **28**, 052001, (2013).
33. J. S. Lee, J. H. Seo, S. Cho, J.-H. Lee, S.-W. Kang, J.-H. Bae et al., "Simulation study on effect of drain underlap in gate-all-around tunneling field-effect transistors," *Current Applied Physics*, **13**, 1143, (2013).
34. K. Nigam, S. Gupta, S. Pandey, P. Kondekar, and D. Sharma, "Controlling the ambipolarity and improvement of RF performance using Gaussian Drain Doped TFET," *International Journal of Electronics*, **105**, 806, (2018).
35. R. Goswami and B. Bhowmick, "Hetero-gate-dielectric gate-drain underlap nanoscale TFET with a δp+ Si 1− x Ge x layer at source-channel tunnel junction," in *2014 International Conference on Green Computing Communication and Electrical Engineering (ICGCCEE)*, 1 (2014).
36. P. Jain, V. Prabhat, and B. Ghosh, "Dual metal-double gate tunnel field effect transistor with mono/hetero dielectric gate material," *Journal of Computational Electronics*, **14**, 537, (2015).
37. *VNL-ATK is a licensed software which can be accessed from: https://docs.quantumwise.com/v2016/*.
38. Q. Pang, Y. Zhang, J.-M. Zhang, V. Ji, and K.-W. Xu, "Electronic and magnetic properties of pristine and chemically functionalized germanene nanoribbons," *Nanoscale*, **3**, 4330, (2011).
39. M. Ali, X. Pi, Y. Liu, and D. Yang, "Electronic and magnetic properties of graphene, silicene and germanene with varying vacancy concentration," *AIP Advances*, **7**, 045308, (2017).
40. P. Sharma, S. Singh, S. Gupta, and I. Kaur, "Modeling linearity and ambipolarity in GFETs on different dielectrics for communication applications," *Journal of Materials Science: Materials in Electronics*, **29**, 2883, (2018).
41. S. Chang, Y. Zhang, Q. Huang, H. Wang, and G. Wang, "Effects of vacancy defects on graphene nanoribbon field effect transistor," *Micro & Nano Letters*, **8**, 816, (2013).
42. L. De Michielis, L. Lattanzio, K. E. Moselund, H. Riel, and A. M. Ionescu, "Tunneling and occupancy probabilities: How do they affect tunnel-FET behavior?," *IEEE Electron Device Letters*, **34**, 726, (2013).
43. L. Liu, D. Mohata, and S. Datta, "Scaling length theory of double-gate interband tunnel field-effect transistors," *IEEE Transactions on Electron Devices*, **59**, 902, (2012).
44. S. Kaneko, H. Tsuchiya, Y. Kamakura, N. Mori, and M. Ogawa, "Theoretical performance estimation of silicene, germanene, and graphene nanoribbon field-effect transistors under ballistic transport," *Applied Physics Express*, **7**, 035102, (2014).
45. D. Dideban, A. Ketabi, M. Vali, A. H. Bayani, and H. Heidari, "Tuning the analog and digital performance of Germanene nanoribbon field effect transistors with engineering the width and geometry of source, channel and drain region in the ballistic regime," *Materials Science in Semiconductor Processing*, **80**, 18, (2018).